JOURNAL OF MATERIALS SCIENCE 39 (2004) 6781–6790

Application of Raman microscopy to the analysis of silicon carbide monofilaments

Y. WARD, R. J. YOUNG
Manchester Materials Science Centre, UMIST/University of Manchester, Manchester M1 7HS, UK
E-mail: robert.young@umist.ac.uk

R. A. SHATWELL
Structures and Materials Centre, QinetiQ, Cody Technology Park, Farnborough, Hants, GU14 0LX

This paper reviews recent research upon the application of Raman microscopy to the characterisation of silicon carbide monofilaments produced by CVD (chemical vapour deposition). It is demonstrated that Raman microscopy is an invaluable technique allowing qualitative information about stoichoimetry variation in silicon carbide monofilaments to be obtained, as it readily detects both crystalline and amorphous carbon and silicon. It is shown that it is possible to characterise the morphology of the SiC crystallites in the monofilaments from analysis of the Raman line shapes. It is also demonstrated that Raman spectroscopy can be used to follow deformation of SiC monofilaments and to determine residual stresses in SiC-monofilament-reinforced metal-matrix composites. In addition, it is shown that it is possible to evaluate internal stresses in the carbon coatings of SiC monofilaments.

1. Introduction

Silicon carbide monofilaments produced by chemical vapour deposition (CVD) technique can achieve much higher levels of strength and stiffness (6 and 420 GPa) when compared with smaller diameter SiC fibres derived from polymer precursors. Their microstructures however, are very sensitive to the detailed conditions of the CVD process [1]. In order to develop strong and tough SiC monofilaments by the CVD process, it is necessary to investigate how the deposition conditions of the CVD process correlate with the composition and microstructure of the monofilaments. This requires quick methods of assessing both the stoichiometry and crystal structure of SiC in the monofilaments.

Raman spectroscopy is a technique involving the inelastic scattering of light. It is in principle a very weak phenomenon with the Raman scattering being typically only 10^{-8} as intense as the conventional Rayleigh scattering. It developed rapidly once lasers became available in the 1960s and it has been applied to a number of problems in physics chemistry and materials science. Raman spectroscopy has been applied successfully to characterise SiC crystal polytypes [2–4], SiC particles [5, 6], and polymer-based SiC fibres [7–9]. The position, relative intensity and bandwidth of Raman spectra are closely related to stacking order (polytypes), crystal size and defects in the structure. The Raman technique also has the advantages of being very quick and efficient, as well as requiring little sample preparation. The microstructure of silicon carbide monofilaments can be examined simply from freshly-fractured surfaces or polished sections of monofilaments.

In the first section, we demonstrate how Raman microscopy can be used as a fast and complementary technique to TEM in assessing composition and microstructure of different CVD silicon carbide monofilaments at the micron scale. It shows that Raman can easily identify the presence of small amounts of carbon and silicon, which could be difficult using electron or X-ray techniques [10]. An analysis of the SiC Raman line shape can also obtain information on the crystal size, the orientation of crystallites and stacking disorder in the structure.

Raman spectroscopy has been proven to be a very powerful method for following the deformation of silicon [11], silicon carbide [12, 13], and carbon fibres [14, 15]. The positions of the Raman bands shift approximately linearly under the application of stress. Earlier work on carbon-containing silicon carbide fibres (Nicalon) produced by polymer precursors [16–18] has also found that the Raman bands due to carbon are sensitive to the levels of strain on the fibre. Hence the deformation behaviour of silicon carbide monofilaments made by the CVD process can be investigated in a similar way as that of carbon fibres and SiC fibres, by following the shift of carbon bands from carbon coating on the monofilaments.

Raman spectroscopy has also been shown as a non-destructive technique to determine the residual strains in unidirectional silicon carbide fibre (Nicalon) reinforced composites by Yang and Young [16], and

Colomban *et al*. [17, 18]. The residual stresses in SiC particulate- and whisker-reinforced Al_2O_3 composites have been measured by DiGregorio *et al*. [6, 13] by means of Raman spectroscopy.

In the second part, we describe how Raman spectroscopy can be used to follow deformation in silicon carbide monofilaments. It is also shown that the stress-induced band shifts from deformation of the monofilaments can be used as a strain gauge to determine both internal stress in the carbon coating on the monofilaments and residual stresses in SiC monofilament reinforced metal-matrix composites.

2. Raman spectroscopy

The silicon carbide monofilaments described in this review are SCS-6, SCS-Ultra and Simga1140+. SCS-type monofilaments, developed by Textron Specialty Materials Co., are produced by chemical vapour deposition onto a 35 μm carbon core are about 140 μm in diameter with a $\sim$3 μm thick coating on the external surface. Sigma 1140+ monofilaments made by QinetiQ, are chemical deposited onto a $\sim$15 μm tungsten core. The Sigma 1140+ monofilaments have a total diameter of $\sim$100 μm and a carbon coating approximately 5 μm thick on the outer surface.

All the Raman spectra were acquired in a back-scattering geometry on a Renishaw 1000 Raman microprobe system, using the 632.8 nm line of a 25 mW He-Ne laser as excitation source.

3. Microstructural characterisation of SiC monofilaments

3.1. Raman spectra of SiC, silicon and carbon

3.1.1. Raman spectra of SiC

Silicon carbide crystallizes in various polytypes with different stacking sequences. The Raman spectra associated with various stacking sequences in SiC are different and so allow polytype identification. Fig. 1 shows Raman spectra of the 3C-, 4H-, and 6H-SiC polytypes in the 300–1100 cm^{-1} region. The position and corresponding symmetry assignment for each band are also shown. The band positions for 3C-, 4H- and 6H-SiC polytypes are consistent with those reported by Feldman *et al*. [2, 3]. The 3C-SiC polytype (β-SiC) exhibits two sharp bands, corresponding to the zone-centre transverse optical phonon (TO) mode at 796 cm^{-1} and the zone-centre longitudinal phonon (LO) mode at 972 cm^{-1} [2, 3]. This splitting arises because all polytypes of SiC have noncentro-symmetric crystalline systems. This gives rise to a long-range electric field within the crystal which increases the energy of the LO phonon mode. The intensity of the band at 796 cm^{-1} is comparable to that of the 972 cm^{-1} in the crystalline, 3C SiC. In the hexagonal polytypes, scattering is only allowed from Brillouin zone-centre phonons with A_1 and E_2 symmetries, when Raman spectra are obtained in a $\{\underline{z}(y, x + y)z\}$ configuration. The E_1(TO) mode at 796 cm^{-1} is symmetry forbidden [3]. The 4H-SiC polytype shows an E_2 (TO) mode at 776 cm^{-1} and an A_1(LO) mode at 977 cm^{-1}· 6H-SiC displays E_2 modes at 766 and 787 cm^{-1} and an A_1(LO) mode at 967 cm^{-1} [2–4]. The LO band in both 4H and 6H polytypes is asymmetric, with a tail to higher energy. This is a function of the local electric fields arising from extrinsic doping of the semiconductor. The LO band broadens and shifts to higher wavenumber as the carrier concentration increases. Raman line shapes of these modes have been used to evaluate carrier concentration in the SiC crystals [19]. In general, it is found that the LO band shows a greater sensitivity to the local environment than the TO bands [2, 3, 5, 7].

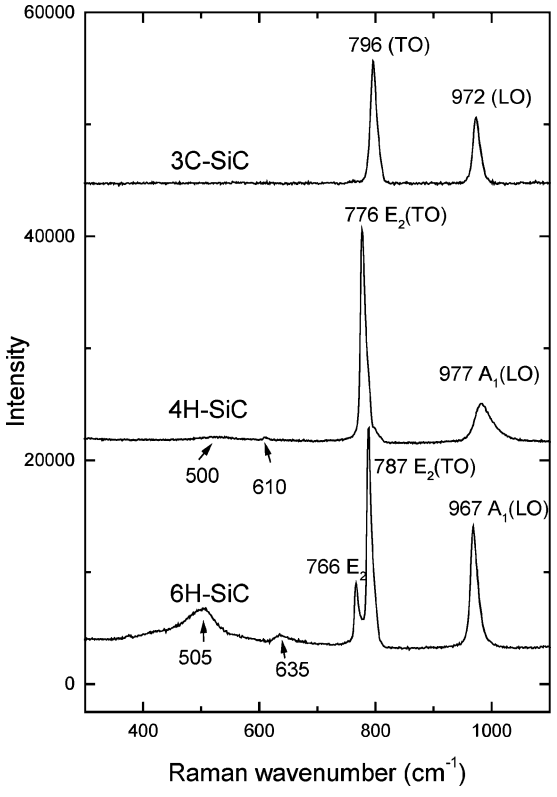

Figure 1 Raman spectra of SiC for 3C-, 4H- and 6H-polytypes. All the spectra were obtained without polarisation selection of the scattered light.

The extra broad bands at 505 and 635 cm^{-1} in 6H-SiC are Raman scattering from electronic excitations in doped SiC, which has been observed in *n*-type SiC by Colwell and Klein [20]. These bands are attributed to a 1s(A_1) to 1s(E) valley-orbit transition at the donor sites [20]. The electronic Raman scattering is sharper at lower temperature [20] and longer excitation wavelength [21].

3.1.2. Raman spectra of silicon

Fig. 2 shows Raman spectra of crystalline silicon and amorphous silicon. Crystalline silicon displays a sharp band at around 520 cm^{-1} that is ascribed to the optical phonon mode of silicon [22]. Unlike SiC, the crystalline form of silicon is centro-symmetric and hence there is no long range electric field to remove the degeneracy of the TO and LO phonons. Amorphous silicon gives rise to a broad band at around 480 cm^{-1} [23, 24].

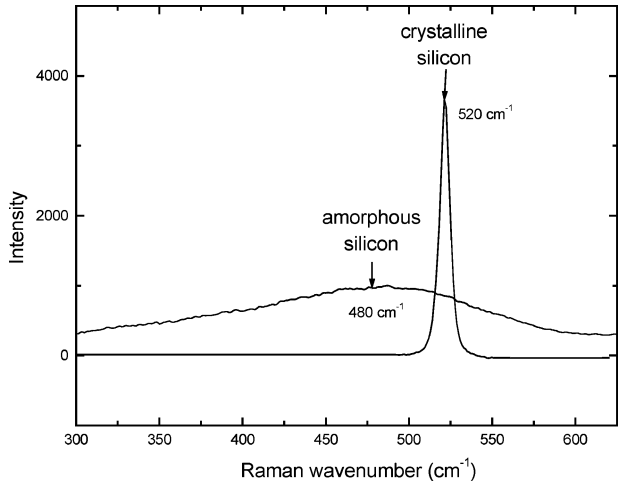

Figure 2 Raman spectra of crystalline and amorphous silicon.

3.1.3. Raman spectra of carbon

Raman spectroscopy has been shown to be a sensitive method for the characterisation of structure of different forms of carbon, ranging from graphite to disordered graphite, amorphous and diamond-like carbon [25–31]. Fig. 3 shows Raman spectra of a number of different carbon fibres, which are similar to the spectrum of disordered graphite. All the spectra show two first-order bands in the 1000–2000 cm^{-1} regions, the G band around 1580–1600 cm^{-1} and the D band at around 1330 cm^{-1}, when the 633 nm line of a He-Ne laser is used. The G band is due to the E_{2g} symmetry in-plane bond stretching of sp^2 carbon and the D band is a Brillouin zone edge phonon and is attributed to the breathing modes of A_{1g} symmetry [25, 29–31]. The D band is forbidden in single crystal graphite and only becomes active in the presence of disorder arising from the crystal boundaries of polycrystalline graphite [25–31]. The D band grows in intensity with increasing disorder or decreasing crystal size in the carbon structure and the ratio of its intensity to that of G band, I_D/I_G, varies inversely with the crystal size of graphitic sheet, L_α [25, 28]. Fig. 3 shows that the positions, relative intensities, and bandwidths of both the D and G bands change with fibre structure. The G band moves from 1580 to 1600 cm^{-1} and the D band increases its intensity relative to the G band as the disorder increases. Disorder in the carbon structure leads to fibres with a lower modulus.

The second-order band at around 2660 cm^{-1} (taken as 2×1330 cm^{-1}) in the 2000–3000 cm^{-1} region can only be observed in carbon fibres of high modulus. While relative intensities of the the first-order bands (D and G) are related to the structural order within the graphitic carbon sheets (two-dimensional ordering), the second-order band intensities are partially dependent on the stacking order along *c*-axis (three-dimensional ordering) [26]. The presence of second-order bands in the Raman spectra reflects the three-dimensional ordering in the graphite structure.

The Raman spectrum of amorphous carbon shows weak and extremely broad D and G bands around 1380 and 1500 cm^{-1}. This is distinctly different from the spectrum of carbon fibres with a disordered graphite structure.

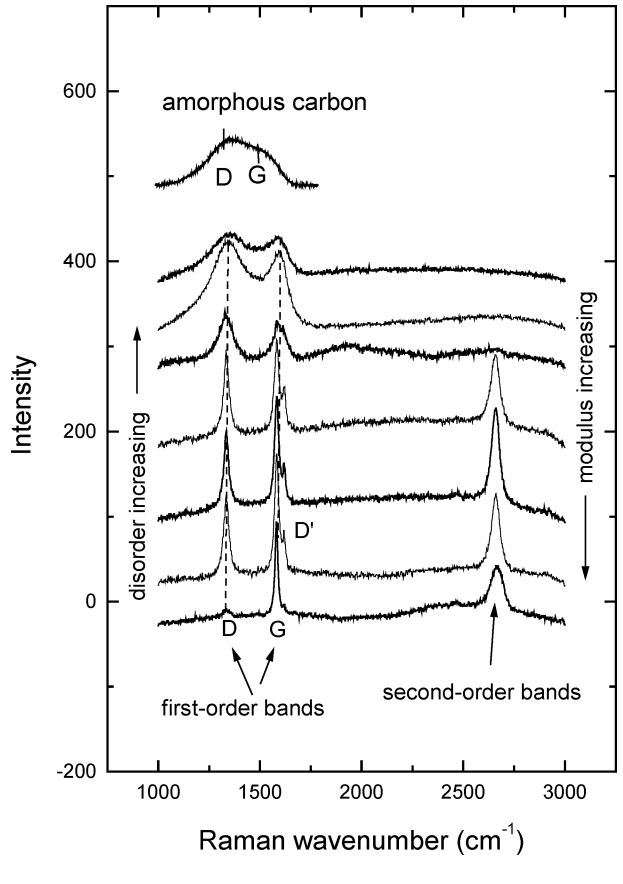

Figure 3 Raman spectra of carbon fibres with different modulus, and amorphous carbon.

3.2. Raman spectra of silicon carbide (SiC) monofilaments

3.2.1. Stoichiometry

Raman spectroscopy has advantages over other techniques for characterising small variations from stoichiometric SiC, as it readily detects both crystalline and amorphous silicon and carbon. The Raman technique was used successfully by Kim *et al.* [32] to detect carbon and silicon in the silicon carbide monofilament SCS-6. A recent study demonstrated that Raman spectroscopy could give detailed information on the stoichiometry of a number of different SiC monofilaments [33].

Fig. 4 displays a series of Raman spectra taken from different positions across the cross-sections of three different types of SiC monofilament. It can be seen that Raman scattering from SiC, silicon and carbon can be easily identified and differentiated. The presence of free carbon in both SCS-6 and SCS-Ultra, gives rise to two bands at around 1330 and 1600 cm^{-1}. The appearance of a broad feature at $\sim$1400 cm^{-1} in SCS-Ultra suggests amorphous carbon whereas the presence of a sharp band at 520 cm^{-1} and a broad band centred at around 480 cm^{-1}, indicates both crystalline and amorphous silicon are present in the SM1140+ monofilament. Raman bands from SiC optical phonon scattering are observed in all three type of monofilament between 600 and 1000 cm^{-1}, showing TO band at $\sim$790 cm^{-1} and LO band at 964 cm^{-1}

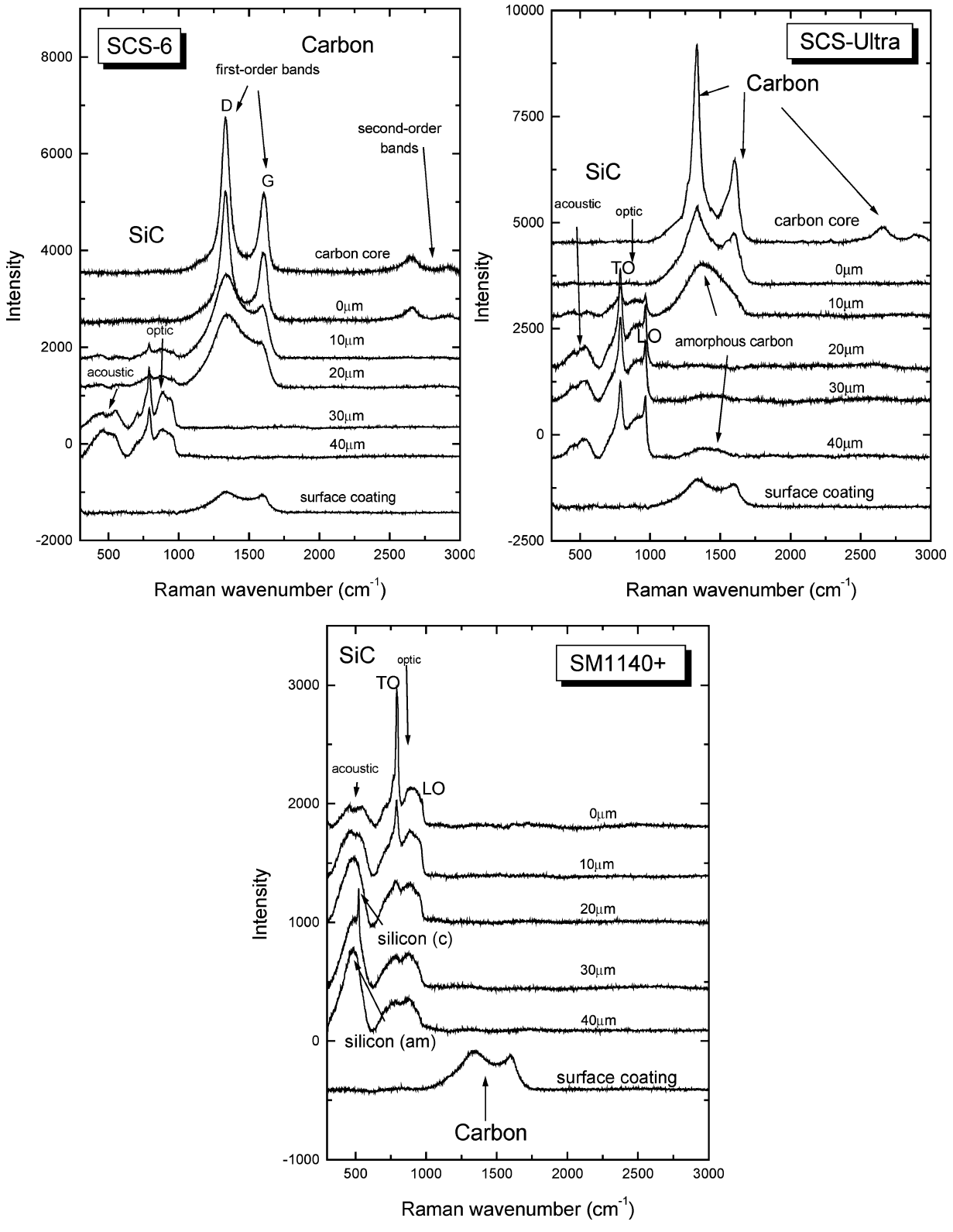

Figure 4 Raman spectra in the 300–3000 cm^{-1} region obtained at different positions across the cross-section of SiC monofilaments: (a) SCS-6, (b) SCS Ultra and (c) Sigma 1140+. For comparison all the spectra have been corrected for background scattering and shifted along the intensity axis.

[2, 3]. The presence of double humps below 600 cm^{-1} is from acoustic phonon scattering of SiC due to disorder in the crystals (grain boundaries, defects and stacking faults) [34]. The Raman spectrum of the SiC near the surface of the SM1140+ monofilament is very similar to that of CVD amorphous SiC [35], which reflects the phonon density of states in the Brillouin zone [22, 34].

Fig. 4 shows that these SiC monofilaments can be carbon-rich, silicon-rich or stoichiometric SiC. The Raman spectra also exhibit specific features associated with crystalline and amorphous SiC, as well as crystalline and amorphous carbon and silicon.

It can be observed that the Raman spectra are not only different from each other but also change with position across the monofilaments. These changes are associated with variations in stoichiometry and microstructure. This indicates that the microstructures in the monofilaments are not uniform because of changing

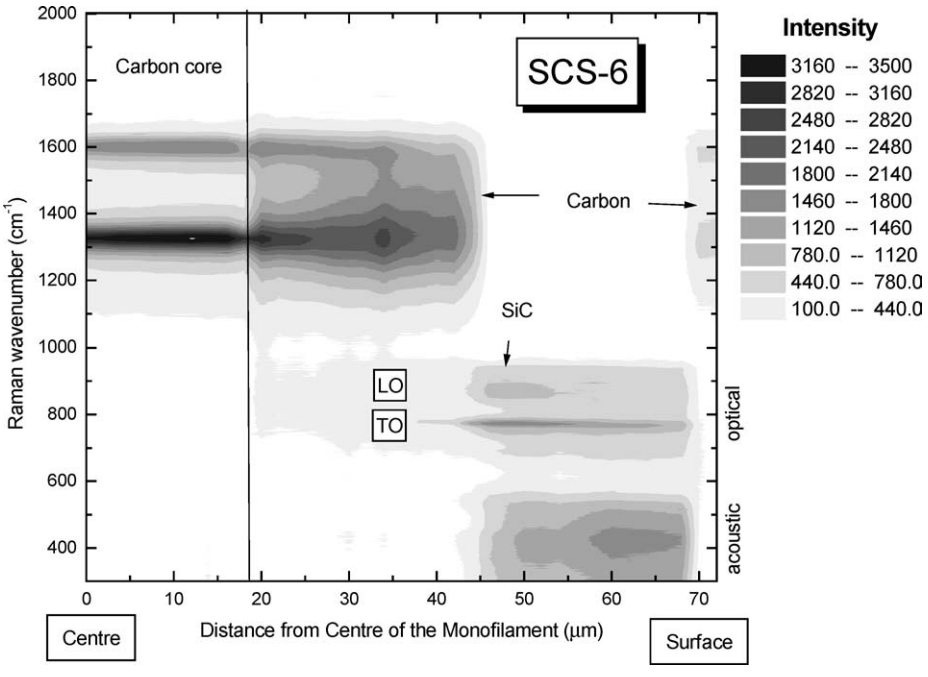

Figure 5 Raman scattering intensity contour map from the centre to the surface of an SCS-6 monofilament.

deposition conditions during growth of SiC monofilaments. The complex microstructure in these monofilaments reflects the importance of their precise characterisation. In recent work [33], the point-to-point variation of Raman spectra at intervals of 2 μm with distance from centre to the surface can be obtained by moving the sample in intervals of 2 μm using an automated $x - y$ stage with a spatial resolution of 1 μm. Such Raman maps can give a visual indication of distribution and form of SiC, carbon and silicon present in the monofilaments.

Fig. 5 shows the Raman mapping of SCS-6 starting from centre of the monofilament. The carbon bands disappear abruptly at a distance about 45 μm away from the centre and reappear of only at very surface (70 μm from the centre) from surface coating. It is clear that the monofilament consists of a graphitic carbon core of 35 μm diameter, an inner region of SiC and carbon of 25 μm thickness and an outer region of stoichiometric SiC about 25 μm thick, followed by a 3 μm carbon coating on the surface.

There is a reduction in relative intensity of carbon to SiC in the inner region. This indicates that there is a subsequent decrease of amount of carbon with distance, as observed by Ning *et al.* [36]. The SiC TO band broadens and shifts towards lower wavenumber from the mid-radius to the surface. This is associated with a decrease in crystal size of SiC as TEM study showed that SiC crystallites are about 250 nm in size around the mid-radius but decrease to only 90 nm near the surface [37].

The microstructure of the SCS-Ultra monofilament is illustrated though the Raman mapping in Fig. 6. The carbon bands disappear at about 35 μm from the centre and re-emerge at around 15 μm from the surface. Thus the SCS-Ultra has three different regions; for the inner and outer regions, a mixture of carbon and silicon carbide, and for the middle region, almost stoichiometric silicon carbide. The outer region contains only a small amount of carbon as going towards the surface. Moving away from the core/SiC boundary, carbon changes from graphitic carbon to more disordered carbon and finally to amorphous carbon. A reduction in relative intensity of carbon to SiC with distance can also be observed. Both the D and G bands in the core show shifts towards higher wavenumber with distance from the centre. This indicates that compressive stresses might be present in the core. Raman scattering from SiC is shown by the sharp and strong TO and LO bands at 790 and 964 cm^{-1}. There appears to be little variation of SiC optical bands with distance, indicating the same SiC crystallite structure across the monofilaments.

Fig. 7 presents the Raman line mapping of Sigma 1140+ monofilament. Carbon bands are absent throughout the entire cross-section except at the very surface from carbon coating. A broad band at $\sim$480 cm^{-1} (rather than the acoustic bands) is observed throughout the entire region, suggestive of amorphous silicon. The 520 cm^{-1} band to crystalline silicon emerges at about 17 μm away from the W core/SiC boundary and is present throughout the outer region. The silicon carbide TO band is very sharp and strong near the W core/SiC boundary but broadens and shifts towards lower wavenumber with distance. The SiC near the surface has an amorphous structure.

The results from Raman maps of the monofilaments illustrate that Raman spectroscopy is a very powerful technique for studying stoichiometry variation in the SiC monofilaments. However, a quantitative analysis of stoichiometry can be difficult due to strong Raman scattering from carbon.

3.3. Microstructure of SiC

Detailed information on the microstructure of SiC crystals can also be obtained from an analysis of

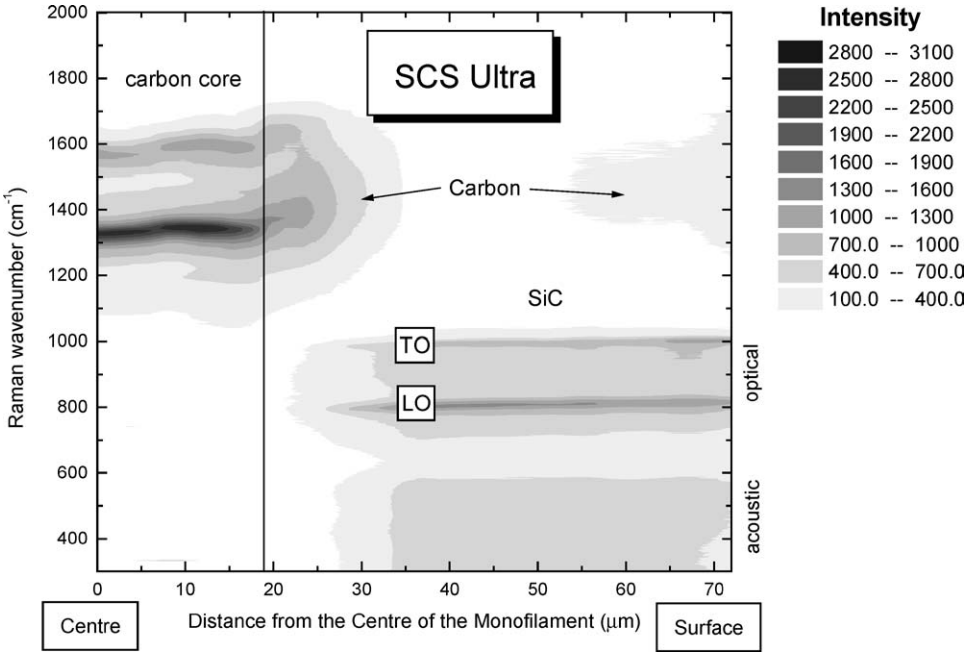

Figure 6 Raman scattering intensity contour map from the centre to the surface of an SCS-Ultra monofilament.

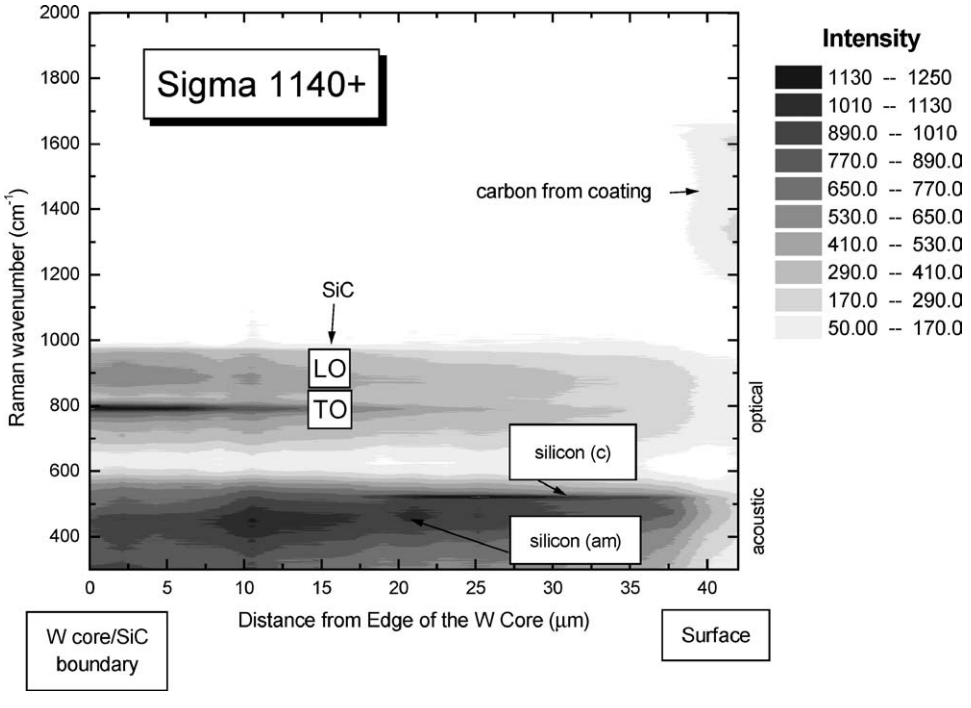

Figure 7 Raman scattering intensity contour map from the W core/SiC boundary to the surface of a Sigma 1140+ monofilament.

the SiC Raman band line shapes. Band shifts, band broadening and relative intensities are closely related to crystal size, orientation of the crystallites and stacking disorder in the SiC crystallites in these monofilaments.

3.3.1. Crystal orientation

The orientation of SiC crystallites in the SiC monofilaments can be determined by means of polarised Raman spectroscopy. The appearance and disappearance of Raman bands or phonon modes with respect to different polarisation geometry can provide valuable information on the crystallite orientation in the monofilaments. SiC optical bands in Figs 5–7 were obtained in a $\{\underline{x}(z, z + y)x\}$ geometry[1], where the z-axis is parallel to the radial direction of the monofilaments. The SiC optical bands of SCS-6 and SM1140+ are similar, showing a strong TO band at 790 cm^{-1}. The LO band at ~970 cm^{-1} is not observed. TEM studies

[1]Damen's notation [38] for the propagation and polarisation configuration has been used. The x, y and z-axes are fixed in the crystal. A four-letter expression, $z(xy)\underline{z}$, consists of a propagation part $z(- -)\underline{z}$ and the polarisation part $-(xy)-$. The part $z(- -)\underline{z}$ means the laser beam incident along the z-axis and is back-scattered along the negative z-axis, and the part $-(xy)-$ means that the polarisation directions of incident and scattered light are along x-and y-axes, respectively.

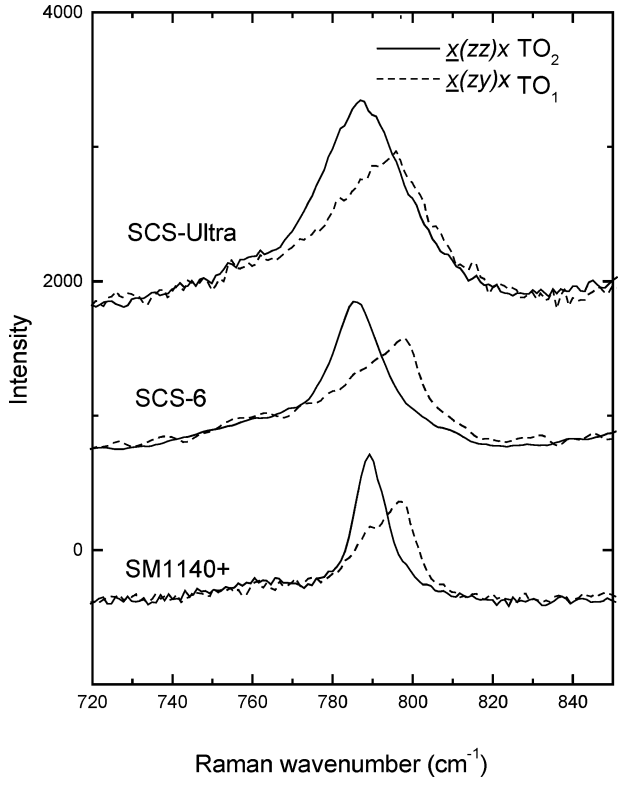

Figure 8 TO_2 bands in a $\{\underline{x}(zz)x\}$ geometry and TO_1 bands in a $\{\underline{x}(zy)x\}$ geometry, for SM1140+, SCS-6 and SCS-Ultra.

show that the SiC crystallites in the monofilaments have a preferential growth direction, the ⟨111⟩ axis parallel to the radial direction. The Raman polarisation data is consistent with this, as it is predicted that only the TO phonon modes should be observed if the laser polarisation is parallel to the ⟨111⟩ direction. In the spectra of SCS-Ultra, both TO and LO bands at 790 and 964 cm^{-1} are observed. This suggests more than one orientation of SiC crystallites. Randomly-oriented SiC crystallites have been observed in the monofilaments of SCS-Ultra by TEM [21].

3.3.2. Stacking faults

SiC optical phonon bands from all three monofilaments demonstrate a considerable amount of Raman scattering from the non-zone-centre phonon of SiC, due to disorder in the crystallites. SiC crystallites in the monofilaments are mainly of the 3C-SiC polytype but are heavily faulted in the radial direction [37, 39]. Stacking faults in 3C-SiC cause a reduction in symmetry from cubic to hexagonal or less, which leads to a splitting of the doubly degenerate TO band into two components, denoted TO_1 and TO_2. The TO_1 peak position is independent of polytype, but the TO_2 peak shifts to lower wavenumber by an amount dependent on the symmetry of the local environment of C or Si atoms. The splitting increases as the hexagonal nature of this environment increases [3, 40, 41] according to:

$$\%h = 3.4\Delta(\mathrm{TO}) \qquad (1)$$

where %h is the percentage of hexagonal character in the local environment and Δ(TO) is the $TO_1 - TO_2$ splitting in cm^{-1}.

It is possible to view the TO_1 and TO_2 components separately by polarised Raman spectroscopy. The TO_2 component can be seen in the $\{\underline{x}(zz)x\}$ and the TO_1 in the $\{\underline{x}(zy)x\}$ orientations. when the laser polarisation is parallel to the radial direction. Fig. 8 shows these two bands. The splitting is about 7 cm^{-1} in SM1140+ and 10 cm^{-1} in SCS-6 and Ultra –SCS. This indicates 24–36% hexagonal character arising from the stacking disorder in the SiC crystallites.

3.3.3. Crystal size

Fig. 9 shows the change in the SiC optical bands for the SM1140+ moving from the W-core/SiC boundary to the surface. It can be seen that SiC TO band broadens and shifts towards lower wavenumber with distance from the core. It has been shown by TEM that the SiC

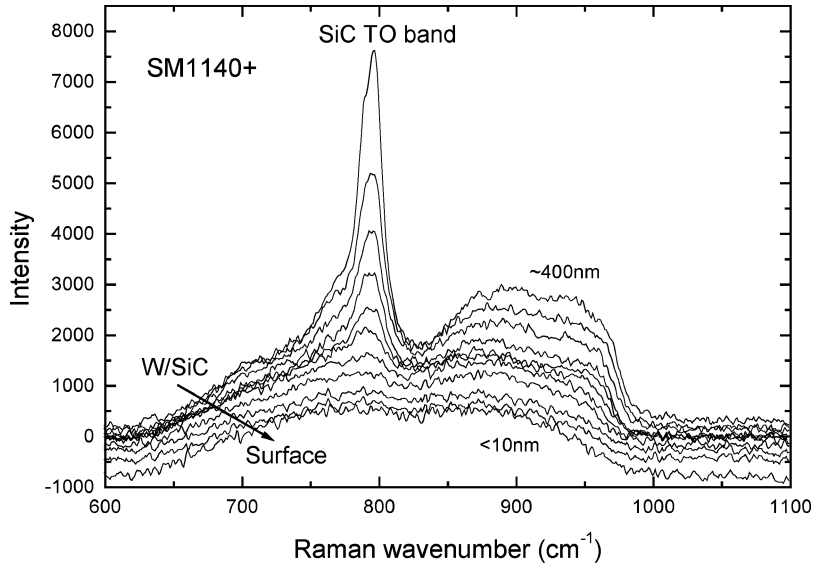

Figure 9 SiC TO bands for the SM1140+, change with distance from W core/SiC boundary to the surface, showing the effect of crystal size on the line shape of SiC TO bands.

crystallites in SM1140+ are ∼400 nm in size near the W/SiC boundary, decreasing in size systematically with distance, and are less than 10 nm near the surface [39]. Thus Fig. 9 reflects the effect of crystal size on the Raman line shapes of the SiC TO bands.

The phonon confinement model developed by Richter *et al*. [22] has been applied successfully to explain the changes in Raman line shape found in microcrystalline silicon and GaAs crystals with damage induced by progressive ion implantation [22, 42]. The model has also been used to explain Raman line shape of SiC optical bands [33]. Lattice imperfection [5] and random stacking fault model [43] have also been developed to account for the changes in the Raman line shape of SiC TO bands. The disorder predicted by all the models may differ in detail but the basic effect is the same in all the models.

In single crystals only phonon modes with wave vector $\mathbf{k} = 0$ contribute to Raman scattering. Reduction in crystal size, or an increase in disorder by defects or stacking faults, leads to a relaxation of $\mathbf{k} = 0$ selection rule, and phonon modes away from the zone centre of the Brilliouin zone contribute to Raman scattering. The TO dispersion curve of 3C-SiC [3, 4] shows that its phonon mode is highest at zone centre, $\mathbf{k} = 0$, and is monotonically reduced towards the zone edge, that is from 797 cm^{-1} at the zone centre to 766 cm^{-1} at the zone edge. The highest phonon mode is observed only in single-crystal 3C-SiC. A progressive relaxation of the $\mathbf{k} = 0$ selection rule with decreasing crystal size leads to a contribution of phonon modes away from the zone centre of lower frequencies. This gives the observed asymmetrical broadening towards lower wavenumbers. Our Raman analysis in Fig. 9 indicates that the broadening of SiC TO band is a refection of a decrease in crystal size.

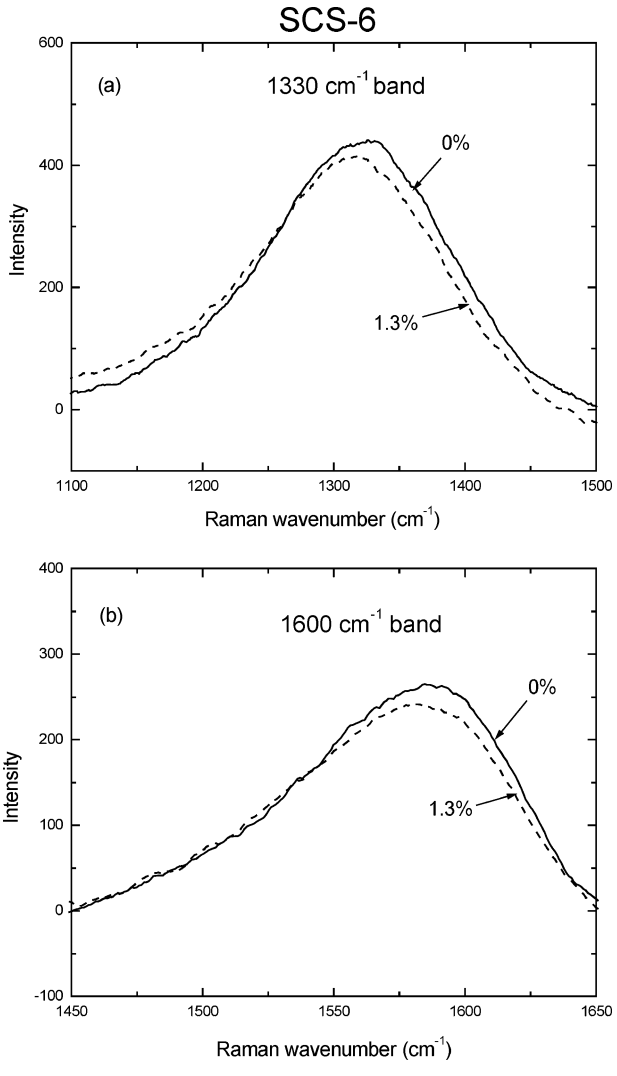

Figure 10 Raman band shifts at (a) 1330 cm^{-1} and (b) 1600 cm^{-1} for an SCS-6 monofilament subjected to a tensile strain of 1.3%.

4. Deformation characterisation of SiC monofilaments

An important application of Raman spectroscopy is its ability to determine stress or strain in a wide range of materials from stress-induced Raman bands shifts. In the following sections, we describe how Raman spectroscopy can be used to measure internal stresses and follow external deformation of SiC monofilaments and of these monofilaments in composites.

4.1. Deformation of SiC monofilaments

Well-defined Raman spectra obtained from the surface of the monofilaments are from the carbon coating since Raman spectroscopy can only detect signals within 1 μm from the surface of SiC or less than 0.1 μm for carbon. Therefore Raman spectra of the surface coatings of the monofilaments (Fig. 4) are similar to those of low-modulus carbon fibres (Fig. 3), showing two main Raman bands; one at 1330 (D band) and the other at 1600 cm^{-1} (G band).

The deformation of monofilaments was carried out by fixing them on the surface of a PMMA beam and subjecting the beam to four-point bending [44]. The deformation behaviour is demonstrated in Fig. 10 for a SiC monofilament subjected to an axial tensile strain of 1.3%. It can be seen that tensile strain causes a considerable shift of both D and G bands towards lower wavenumber. The shift of both the D (1330 cm^{-1}) and G (1600 cm^{-1}) bands as a function of strain in tension is shown in Fig. 11. It demonstrates that the shift of the Raman band position has an approximately linear relationship with the level of applied strain. The strain dependence of Raman band shifts, $(d\Delta\nu/d\varepsilon)$, are found to be approximately -2.6 ± 0.4 cm^{-1}/% strain for the D band and $-1.8\ \pm0.3$ cm^{-1}/% strain for the G band, for a monofilament with an axial coating modulus of about 100 GPa. It has been found that the value of strain-induced band shift, $(d\Delta\nu/d\varepsilon)$ for the G (1600 cm^{-1}) band is proportional to the axial modulus of carbon fibres. This corresponds to a stress-induced band shift of about -1.8 cm^{-1}/GPa for the G band, independent of modulus [15]. Thus the -1.8 ± 0.3 cm^{-1}/% strain shift shown for the G-band in Fig. 11 is consistent with the carbon coating having a modulus of 100 GPa.

The phenomenon of the strain dependence of Raman band shift shown in Fig. 11 for the SiC monofilaments can be used as an optical strain gauge for the determination of strain or stress distribution in composites reinforced with the same SiC monofilaments.

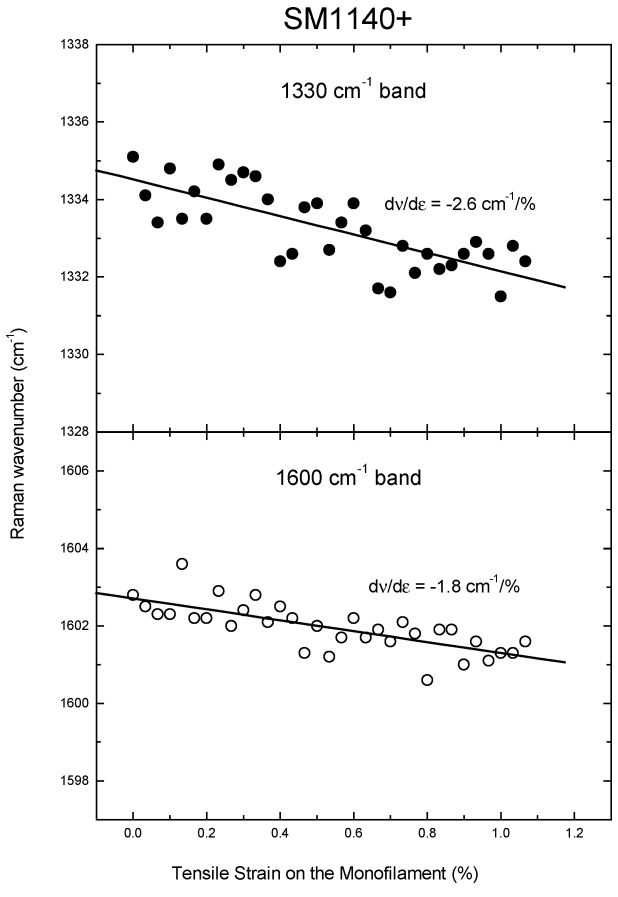

Figure 11 Shifts in position of the Raman bands at (a) 1330 cm^{-1} and (b) 1600 cm^{-1} with tensile strains for a Sigma 1140+ monofilament. The straight lines are the linear least-square fits to the data.

4.2. Residual stresses in composites

Residual stresses usually build up in composites on cooling down from high fabrication temperatures due to a mismatch in thermal expansion coefficient between the monofilament and the matrix. Since well-defined Raman spectra can also be obtained from the carbon coating on the monofilaments embedded within the composites, it is possible to use Raman spectroscopy to determine thermal residual stresses in SiC monofilament-reinforced metal-matrix composites [44].

Ward and coworkers [44] undertook a detailed study of using Raman spectroscopy to determine the magnitude of the internal stresses in metal-matrix composites consisting of SiC monofilaments in a titanium alloy matrix. Raman spectra were obtained from both ends and middle of monofilaments in the composites, from longitudinal sections of the composites with the laser beam polarised parallel to the axial direction for all the measurements. The difference observed in the band positions between the ends and middle of the monofilaments within the composites is due to residual stress in the composites. Both the 1330 and 1600 cm^{-1} bands in the composites are found to shift to higher wavenumber. Since tensile deformation causes the shift of both bands towards lower wavenumber, a shift towards higher wavenumber indicates that the SiC monofilaments within composites are subjected to compression. The Raman band shifts, $d\Delta\nu$, determined from the difference in band position between the monofilament ends and monofilaments in the composites were about $+1.4$ cm^{-1} (D band) and $+0.8$ cm^{-1} (G band) for the SM1140+ composites. Using strain-induced band shift in Fig. 11 and an axial coating modulus of 100 GPa, the axial residual stress was estimated to be around -590 MPa for a 30 vol% Sigma1140+/Ti-6Al-4V composite. This level of axial residual stress measured from the Raman band shift is in good agreement with theoretical prediction based on the continuous coaxial cylinder model of Warwick and Clyne [45].

4.3. Internal stresses in the carbon coating

The point-to-point variation of stress along the monofilament away from the broken ends can be determined from the measurements of position of carbon bands using the strain-induced band shifts. Fig. 12 shows point-to-point stress distribution of carbon coating along an SM1140+ monofilament,

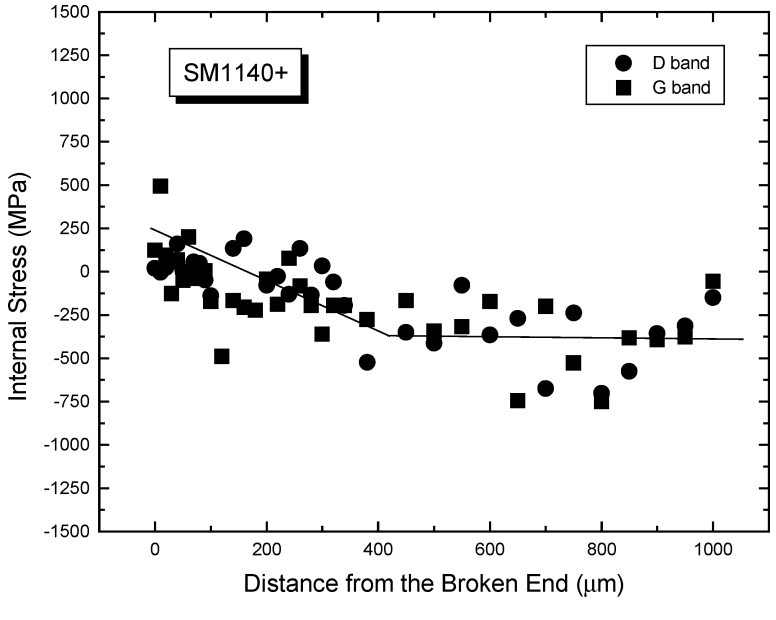

Figure 12 Stress distribution measured along the axial direction as a function of distance from the broken end of an SM1140+ monofilament.

without external deformation on the monofilaments. It demonstrates that there is considerable internal stress in the carbon coating of SM1140+ monofilaments. The stress in the coating varies systematically along the length of the monofilament. The stress builds up from the broken ends with distance along the monofilaments and finally reaches a saturation value at approximately 400 μm. The stress distribution in the carbon coating along an SM1140+ monofilament is similar to the conventional shear lag analysis used in composites [46]. It can be seen that the middle of the monofilament is subjected to a compressive stress of around -400 MPa. This is due to internal stress induced in the CVD process, caused by thermal mismatch between the carbon coating and SiC substrate. Axial thermal expansion coefficient of carbon (0.5×10^{-6} K^{-1}) is much lower than that of the SiC substrate (4.2×10^{-6} K^{-1}), which leads to compressive residual stresses in the carbon coating on cooling. The axial residual stress in the carbon coating of SM1140+ monofilament is estimated to be about -390 to -410 MPa from the Raman band shifts. Fig. 12 also shows that the transfer length over which the stress builds up is almost 400 μm for the coated SM1140+ monofilaments. This indicates a weak bond between the carbon coating and SiC, as required for good axial strength in composites.

References

1. P. MARTINEAU, M. LAHAYE, R. PAILLER, R. NASLAIN, M. COUZI and F. CRUEGE, *J. Mater. Sci.* **19** (1984) 2731.
2. D. W. FELDMAN, J. H. PARKER, JR, W. J. CHOYKE and L. PATRICK, *Phys. Rev.* **170** (1968) 698.
3. *Idem.*, *ibid.* **173** (1968) 787.
4. S. NAKASHIMA and H. HARIMA, *Phys. Stat. Sol.* (a) **162** (1997) 39.
5. Y. SASAKI, Y. NISHINA, M. SATO and K. OKAMURA, *Phys. Rev.* **40** (1989) 1762.
6. J. F. DIGREGORIO and T. E. FURTAK, *J. Amer. Ceram. Soc.* **75** (1192) 1854.
7. Y. SASAKI, Y. NISHINA, M. SATO and K. OKAMURA, *J. Mater. Sci.* **22** (1987) 443.
8. R. J. DAY, V. PIDDOCK, R. TAYLOR, R. J. YOUNG and M. ZAKIKHANI, *ibid.* **24** (1989) 2898.
9. S. KARLIN and PH. COLOMBAN, *J. Raman Spectr.* **28** (1997) 219.
10. R. T. BHATT and D. R. HULL, *Ceram. Engng. Sci. Proc.* **12** (1991) 1832.
11. E. ANASTASSAKIS, A. PINCZUK and E. BURSTEIN, *Solid State Commun.* **8** (1970) 133.
12. D. OLEGO, M. CARDONA and P. VOGEL, *Phys. Rev.* B **25** (1982) 3878.
13. J. F. DIGREGORIO, T. E. FURTAK and J. J. PETROVIC, *J. Appl. Phys.* **71** (1992) 3524.
14. N. MELANITIS and G. GALIOTIS, *J. Mater. Sci.* **25** (1990) 5081.
15. Y. HUANG and R. J. YOUNG, *Carbon* **33** (1995) 97.
16. X. YANG and R. J. YOUNG, *Brit. Ceram. J.* **93** (1994) 1.
17. G. GOUADEC, S. KARLIN and Ph. COLOMBAN, *Composites* B **29** (1998) 251.
18. R. J. YOUNG. A. BROADBRIDGE and S. L. SO, *J. Microscopy* **196** (1999) 257.
19. H. HARIMA, S. NAKASHIMA and T. UEMURA, *J. Appl. Phys.* **78** (1995) 1996.
20. P. J. COLWELL and M. V. KLEIN, *Phys. Rev.* **6** (1972) 498.
21. Y. WARD and R. J. YOUNG, (unpublished results).
22. H. RICHTER, Z. P. WANG and L. LEY, *Solid State Commun.* **39** (1981) 625.
23. T. TANAKA, E. MARUYAMA, T. SHIMADA and H. OKAMOTO, "Amorphous Silicon" (John Wiley & Sons Ltd., Chichester, 1999) p. 78.
24. Z. IQBAL, S. VEPREK, A. P. WEBB and P. CAPEZZUTO, *Solid State Commun.* **37** (1981) 993.
25. F. TUINSTRA and J. L. KOENIG, *J. Chem. Phys.* **53** (1970) 1126.
26. C. CHIEN, G. DRESSELHAUS and M. ENDO, *Phys. Rev.* B **26** (1982) 5867.
27. N. H. CHO, K. M. KRISHNAN, D. K. VEIRS, M. D. RUBIN, C. B. HOPPER, B. BHUSHAN and D. B. BOGY, *J. Mater. Res.* **5** (1990) 2543.
28. D. S. KNIGHT and W. B. WHITE, *ibid.* **4** (1989) 385.
29. A. C. FERRARI and J. ROBERTSON, *Phys. Rev.* B **61** (2000) 14095.
30. *Idem.*, *ibid.* B **65** (2001) 1762.
31. I. POCSIK, M. HUNDHAUSEN, M. KOOS and L. LEY, *J. Non. Cryst. Solids.* **227–230** (1998) 1083.
32. J. KIM, S. TLALI, H. E. JACKSON, J. E. WEBB and R. N. SINGH, *J. Appl. Phys.* **82** (1997) 407.
33. Y. WARD, R. J. YOUNG and R. SHATWELL, *J. Mater. Sci.* **36** (2001) 55.
34. M. H. BRODSKY and M. CARDONA, *J. Non. Cryst. Solids.* **31** (1978) 81.
35. T. KRAFT, K.G. NICKEL and Y.G. GOGOTSI, *J. Mater. Sci.* **33** (1998) 4357.
36. X. J. NING, P. PIROUZ and S. C. FARMER, *J. Amer. Ceram. Soc.* **76** (1993) 2033.
37. X. J. NING and P. PIROUZ, *J. Mater. Res.* **6** (1991) 2234.
38. T. C. DAMEN, S. P. S. PORTO and B. TELL, *Phys. Rev.* **142** (1966) 570.
39. T. T. CHENG, I. P. JONES, R. A. SHATWELL and P. DOORBAR, *Mater. Sci. Eng.* A **260** (1999) 139.
40. S. NAKASHIMA, H. OHTA, M. HANGYO and B. BALOSZ, *Philos. Mag.* B **70** (1994) 971.
41. R. SHATWELL, K. L. DYOS, C. PRENTICE, Y. WARD and R. J. YOUNG, *J. Microscopy* **201** (2001) 179.
42. K. K. TIONG, P. M. AMIRTHARAJ and F. H. POLLAK, *Appl. Phys. Lett.* **44** (1984) 122.
43. S. ROHMFELD, M. HUNDHAUSEN and L. LEY, *Phys. Rev.* **58** (1998) 9858.
44. Y. WARD, R. J. YOUNG and R. A SHATWELL, *Composites* A **33** (2002) 1409.
45. C. M. WARWICK and T. W. CLYNE, *J. Mater. Sci.* **26** (1991) 3817.
46. H. L. COX, *Brit. J. Appl. Phys.* **3** (1952) 72.

Received 29 September 2003
and accepted 20 January 2004